DISCRIMINATING BETWEEN WATER AND ICE CLOUDS USING NEAR-INFRARED AVIRIS MEASUREMENTS

Wouter H. Knap,[1] Piet Stammes,[1] and Robert B. A. Koelemeijer[1]

1. INTRODUCTION

The accuracy of satellite retrievals of cloud parameters, such as particle size and optical thickness, depends strongly on the assumed particle shape in radiative transfer models. Since the single scattering properties of water droplets and ice crystals are very different (see e.g. Mishchenko et al., 1996), it is essential to know if one is dealing with water clouds or ice clouds, prior to retrieving cloud parameters. In fact, discrimination between water and ice clouds should be regarded as the first step in schemes designed for the retrieval of cloud properties from satellite measurements.

In the present study we investigate the possibility of using spectral measurements of reflected cloud radiance for distinguishing between water and ice clouds. The analysis is part of a scientific project named "Cloud Absorption Retrieval using the near-IR channels of SCIAMACHY" (CARIS). SCIAMACHY is an acronym for SCanning Imaging Absorption spectroMeter for Atmospheric ChartographY[2]. This spectrometer has been designed for measuring radiances in the ultraviolet, visible, and near-infrared wavelength regions (240-2380 nm) at moderate spectral resolution (0.2-1.5 nm). It will be flown on ESA's ENVISAT, which is planned to be launched in 2001. The mission objectives of SCIAMACHY are mainly defined in the area of atmospheric chemistry. CARIS, however, focusses entirely on the design of algorithms for the retrieval of cloud properties. In an earlier stage of the project the use of imperfect hexagonal ice crystals (Hess et al., 1998) for the retrieval of cirrus properties has been studied (Knap et al., 1999).

In this paper we exploit differences in the absorption spectra of water and ice around 1.6 μm to develop a water/ice cloud discrimination algorithm on the basis of near-infared top-of-atmosphere reflectivities. Differences in near-infrared spectra of water and ice clouds have been mentioned in earlier literature (Pilewskie and Twomey, 1987a; Pilewskie and Twomey, 1987b). However, a detailed analysis of reflectivity spectra around 1.6 μm of water and ice clouds on the basis of both model calculations and spectral measurements has not been presented before, as far as we know. Pending SCIAMACHY measurements, we apply our algorithm to AVIRIS measurements made under cloudy conditions over the Pacific Ocean. Since AVIRIS and SCIAMACHY have comparable spectral coverages, we expect to benefit from the analysis presented here when SCIAMACHY measurements become available.

2. MODEL CALCULATIONS

The basis of our method of distinguishing between water and ice clouds is the imaginary part of the refractive index, *Im(m)*, of water and ice (Figure 1a). We examined the absorption spectra for wavelengths λ where (1) the atmosphere is relatively transparant for gaseous absorption, and (2) the slope $dIm(m)/d\lambda$ for water is significantly different from the slope for ice. Condition (1) needs to be satisfied because absorption by atmospheric gases should affect as little as possible the signal originating from clouds and measured by a satellite or aircraft instrument. Condition (2) makes the method independent on the absolute radiance level measured, and thus independent on solar and viewing geometry and radiometric instrument calibration. With these conditions in mind we selected the wavelength region between 1.6 and 1.7 μm, where the atmosphere is transparant for water vapour, and where *Im(m)* has a local minimum for water and a steep slope for ice (close-up: Figure 1b).

The purpose of the present section is to present simulations of cloud spectra of typical water and ice clouds. To do so, we defined two model clouds: a water cloud consisting of spherical water droplets (effective radius: 10 μm) and an ice cloud consisting of imperfect hexagonal ice crystals (length: 60 μm, diameter: 44 μm). The term "imperfect" refers to a certain degree of small-scale roughness at the crystal surface. The single scattering properties

[1] Royal Netherlands Meteorological Institite (KNMI), PO Box 201, 3730 AE De Bilt, The Netherlands, e-mail: knap@knmi.nl.
[2] Detailed information on SCIAMACHY can be found on http://www.sron.nl or http:/www.iup.physik.uni-bremen.de.

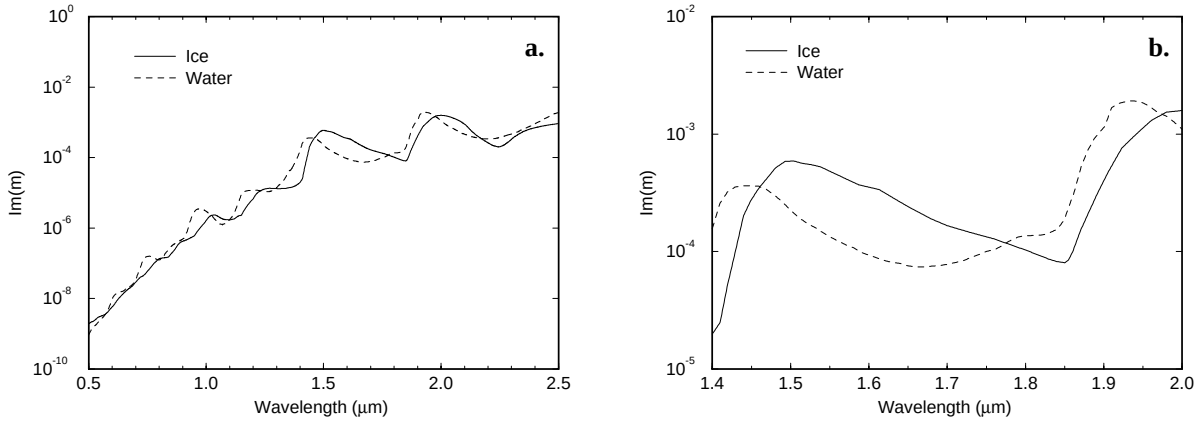

Fig. 1. (a) Imaginary part of the refractive index, Im(m), of ice and water as a function of wavelength between 500 and 2500 nm and **(b)** between 1400 and 2000 nm. Sources: Hale and Querry (1973), Palmer and Williams (1974), and Downing and Williams (1975) for water, and Warren (1984) for ice.

of these crystals were calculated by means of ray-tracing techniques. Further details on imperfect ice crystals and their single scattering properties can be found in Hess et al. (1998). The single scattering properties of water droplets were calculated using Mie theory. The calculations for multiple scattering of sunlight in a cloudy atmosphere were performed with the Doubling-Adding KNMI (DAK) model (Stammes, 1994). The model consists of a plane-parallel atmosphere over a Lambertian surface with prescribed surface albedo (A_s). Since the AVIRIS measurements were made over ocean (see Section 3) we took for A_s a relative low value (0.03, wavelength independent). The model atmosphere containes neither aerosols nor absorbing gases.

Figure 2 shows modelled spectra of top-of-atmosphere nadir reflectivity (R_m) for the two cloud types described above. The optical thickness of both clouds is set to 10 and the solar zentih angle is 30°. According to this figure, many of the features seen in *Im(m)* of water and ice (Figure 1b) are found again (in reversed sense) in the modelled reflectivity spectra of water and ice clouds. Figure 1b shows that slope of R_m at 1.68 μm (denoted by S_m) is about 0 for the water cloud and at its maximum for the ice cloud. To further investigate the relationship between various cloud properties and S_m, we performed several sensitivity experiments that will be described in turn. For these experiments we approximate S_m as follows: $S_m \approx [R_m\,(1.70\ \mu m) - R_m\,(1.65\ \mu m)] / 0.05$ (unit: μm^{-1}). The results are summarized in Figures 3a-d.

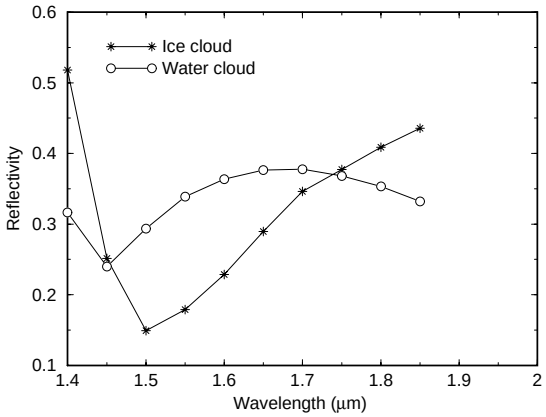

Fig. 2. Model calculations of top-of-atmosphere nadir reflectivity R_m as a function of wavelength, for an atmosphere with an ice cloud consisting of imperfect hexagonal ice columns (length: 60 μm, diameter: 44 μm), and for an atmosphere with a water cloud consisting of spheres (effective radius: 10 μm). For both clouds the optical thickness is 10. The model atmosphere contains neither aerosols nor absorbing gase. The solar zenith angle is 30°. The surface albedo is 0.03, corresponding to a water surface.

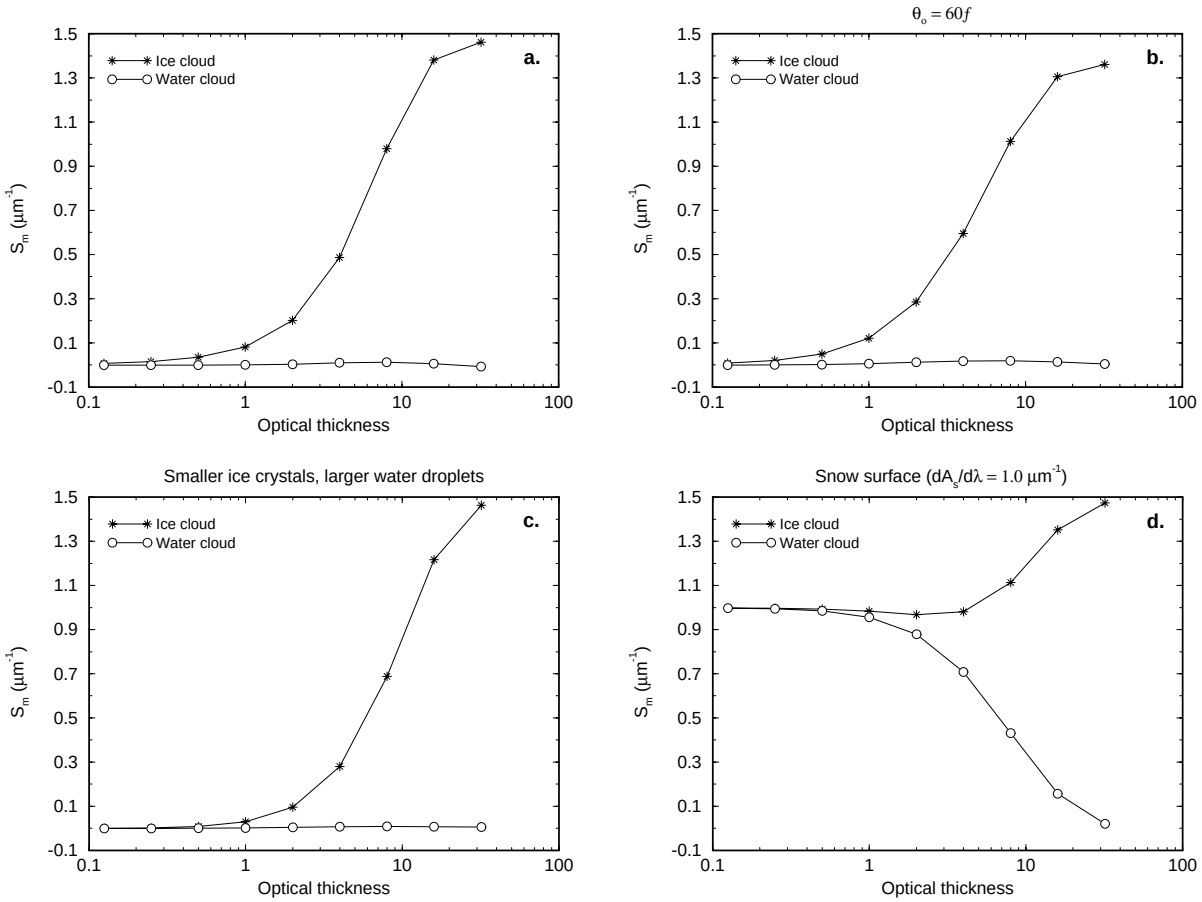

Fig. 3 (a) Modelled slope in the reflectivity at 1.68 μm (S_m) as a function of cloud optical thickness for the same cloudy atmosperes as in Figure 2 (θ_o = 30° and nadir viewing), **(b)** for θ_o = 60°, **(c)**, for a water cloud consisting of larger water droplets (radius: 15 μm) and for an ice cloud consisting of smaller ice crystals (length: 30 μm, diameter: 20 μm), **(d)** for a snow surface.

Cloud optical thickness τ

Figure 3a shows S_m as function of τ for the two average cloudy atmospheres. For the ice cloud, S_m shows asymptotic behaviour at the two extremes of cloud optical thickness: for an optically thin cloud S_m approaches the surface value ($S_m \rightarrow 0$ for $\tau \rightarrow 0$) and for an optically thick cloud the spectral signature of the surface has negligible influence on the cloud spectrum ($S_m \rightarrow$ constant for $\tau \rightarrow \infty$). For τ between 1 and 10, S_m increases rapidly with τ, which implies that as the ice cloud becomes optically thicker the contrast with the water cloud becomes larger. The figure suggests that it is possible to define some threshold T (e.g. T = 0.1 μm^{-1} or even smaller) which marks the transition from water cloud ($S_m < T$) to ice cloud ($S_m > T$). Since $S_m \approx 0$ for both a water cloud and a clear atmosphere over a water surface, these two cases cannot be distinguished from each other using the spectral slope. This problem can be solved by including the reflectivity itself in the analysis; the cloudy atmosphere is much brighter than the underlying sea surface. We will come back to this point when discussing the AVIRIS measurements (Section 3).

Solar zenith angle θ_o

In order to study the effect of changing θ_o, we repeated the calculations shown in Figure 3a with θ_o = 60° instead of θ_o = 30° (Figure 3b). This change has little effect which suggests that S_m might be insensitive for changes in the scattering angle. Obviously, a broader range of scattering angles needs to be considered before conclusions can be drawn.

Cloud particle size

In order to investigate whether the contrast in S_m for water and ice clouds is sensitive to changes in the cloud particle size, we increased the droplet radius to 15 μm and decreased the crystal size to 30 μm in length and 20 μm in

diameter. With respect to the absorbing volume of the cloud particles, this exercise increases the similarity between the water cloud and the ice cloud. Again, this experiment has little effect which suggests that S_m may be insensitive to variations in droplet size and crystal size.

Surface albedo A_s

Figure 3d shows simulations for the same clouds as in Figure 3a, but for a surface with $A_s = 0.35$ at $\lambda = 1.70$ μm and with a spectral slope $dA_s/d\lambda = 1.0$ μm^{-1}. These values more or less correspond to a snow pack consisting of fine grains (larger grains lead to a smaller slope; Wiscombe and Warren, 1980). As in the case of a spectrally neutral surface, S_m varies between the surface and cloud values. The water cloud and the ice cloud are equally well distinguishable, but the contrast between the ice cloud and the surface is smaller, especially for small cloud optical thickness. On the other hand, there is now a strong contrast between the water cloud and the surface.

Because of the presence of liquid water in leaves and organic material, many natural ground surfaces, like vegetation and soil, have values of $dA_s/d\lambda$ close to 0 (see Bowker et al., 1985). This implies that for clouds over these surfaces the situation is very much similar to the one of clouds over a water surface (Figure 1a), even though the surface albedo may be quite different. The slope of 1.0 μm^{-1} in the spectral surface albedo of snow seems to be the upper limit for natural surfaces. This would imply that for clouds over natural surfaces, S_m (for $\tau \to 0$) may vary between 0 and about 1.0 μm^{-1}, and that Figures 3a and 3d represent the extreme cases.

3 AVIRIS MEASUREMENTS

In order to evaluate the model calculations presented in the previous section we selected three AVIRIS flight lines, one of which is analyzed in this paper (No. 950602C0101, Figure 4). The header file, which comes with the data and gives general information about the flight line, states that the flight line contains "Cirrus over water with Stratus, followed by Cirrus over water". The broken structure in the clouds in the lower part of the image may suggest the presence of Stratocumulus instead of Stratus. This distinction is not so important; the value of the image is found in the fact that it contains fields of both low-level and high-level clouds which, most probably, consist of water droplets and ice crystals, respectively. The entire flight line has been acquired over open ocean.

For the analysis presented here we selected three square areas of 31 × 31 pixels (~ 600 m × 600 m) and two transects of 500 × 10 pixels (~10 km × 0.2 km) and 1000 × 10 pixels (~20 km × 0.2 km). In Figure 4 these areas are indicated by "Sc", "Ci", "Clear", Transect A, and Transect B, respectively. The first two areas are, with respect to reflectivity, relatively homogeneous and contain optically thick Stratocumulus (Sc) and Cirrus (Ci). The third area contains no clouds at all. Transect A extends over gradually thickening and thinning Ci, whereas Transect B contains both Sc and Ci of variable

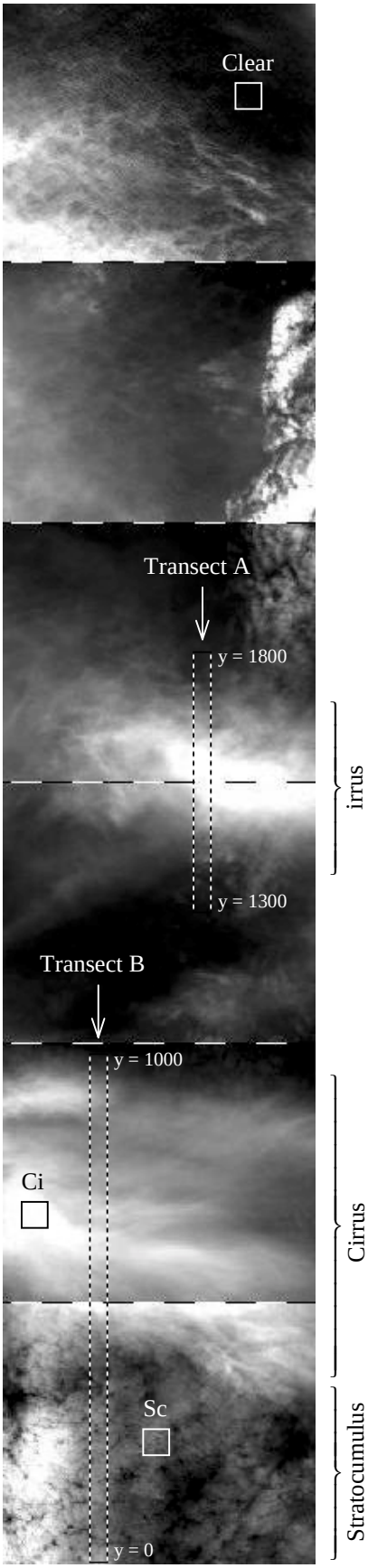

Fig. 4. AVIRIS flight line 950602C0101, site name "Cloud Data". The flight line has been acquired over the Pacific Ocean (48°N, 128°W), about 300 km west of Port Angeles, Washington, USA. The solar zenith angle at the time of the overpass is 31°. For the analysis presented here two homogeneous cloud fields ("Ci" and "Sc") and one clear area ("Clear") are selected. Transect A extends over gradually thickening and thinning Ci, whereas Transect B contains both Sc and Ci of variable optical thickness.

optical thickness. For each pixel of these areas the AVIRIS spectral reflectivity R_A was calculated according to:

$$R_A = \frac{\pi L_A}{S_o \cos\theta_o}. \tag{1}$$

where L_A is the calibrated AVIRIS radiance (W m^{-2} sr^{-1} nm^{-1}) following from the raw image data and the multiplication factors for radiometric calibration that are supplied with the data. S_o is the convolution of the solar spectrum and the AVIRIS slit function, which is approximated by a Gaussian function (standard deviation supplied with the data).

3.1 Analysis of spectra

Figure 5a shows area-averaged spectra of the Sc and Ci fields and, for comparison, of the Clear area. The absorption bands of gases such as O_2 and H_2O can clearly be recognized by strong reductions in cloud reflectivity. For the shorter wavelengths the ice cloud is significantly brighter than the water cloud, which may be explained by the fact that ice crystals scatter more radiation in the sideward direction than water droplets. It is worth mentioning that the water-cloud reflectivity is substantially larger in the lower left corner of the image (Figure 4). This area proves to correspond to scattering angles around 135°, which indicates that AVIRIS looks into the cloudbow. Note that the strong increase in reflectivity for these scattering angles confirms that we are dealing with a water cloud. For the longer wavelengths, absorption instead of scattering is the dominant process that determines cloud reflectivity in the atmospheric windows. This means that absorption features of water and ice should show up in the reflectivity spectrum, as was predicted in the previous section. The spectrum between 1.4 and 2.0 μm shows that this is indeed the case (cf. Figure 5b with Figures 2 and 1b); the wavelength shift in *Im(m)* and R_m is clearly present in R_A. This implies that the principle of using the shape of the reflectivity spectrum around 1.68 μm for discriminating between water and ice clouds is basically correct.

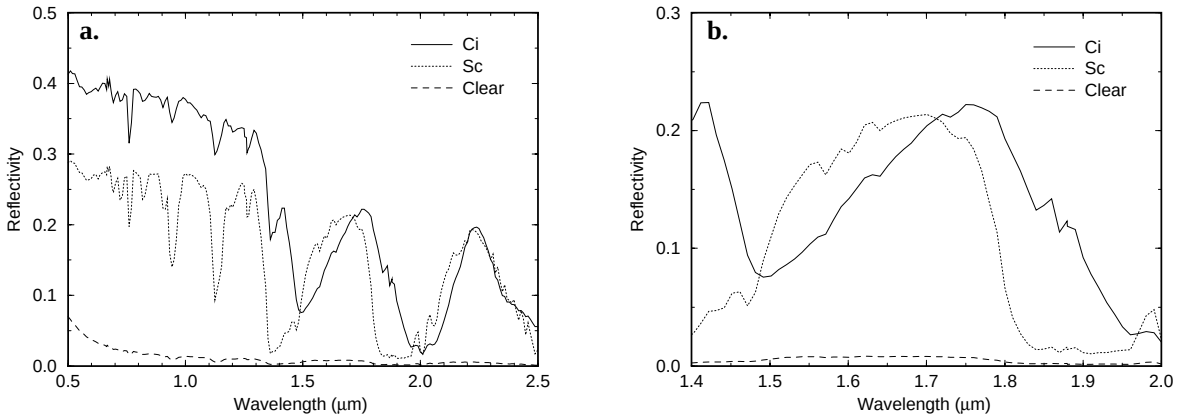

Fig. 5: (a) Mean AVIRIS spectra for the Sc and Ci fields, and for the clear area (location indicated in Figure 4). Each spectrum is the average of 31 × 31 pixels, which corresponds to an area of about 600 × 600 m^2. **(b)** A close-up view of **(a)**.

The irregularities in the cloud spectra for wavelengths around 1.6 μm (Figure 5b), which are caused by CO_2 absorption, interfere with the determination of the spectral slope S_A at 1.68 μm. In order to remove the CO_2 absorption features we applied a 7-point running mean to smooth the cloud spectra. Differentiation at 1.68 μm (in practise: at the nearest AVIRIS wavelength) was performed using 3-point Lagrangian interpolation. Histograms of S_A for the Sc and Ci fields and the clear area are shown in Figure 6. The separation between water and ice cloud is obvious: S_A for the Sc field peaks at values close to 0 (average: 0.01 μm^{-1}) whereas S_A for the Ci field peaks at an average value of 0.61 μm^{-1}. Since the distributions do not overlap, the phase (water/ice) of a cloudy pixel in this selection of measurements can unambiguously be established on the basis of the magnitude of S_A. Discrimination between the Sc field and the clear area is problematic because S_A is close to 0 for both areas and the distributions

partly overlap. The slightly positive value of S_A for the Sc field may be due to the presence of optically thin Cirrus, but it is also possible that it is an artifact of the method of determining S_A. Since S_A is not a good criterion for discriminating between the water cloud and the water surface, R_A itself may be used to identify the water cloud. Obviously, this only works for a dark surface such as water.

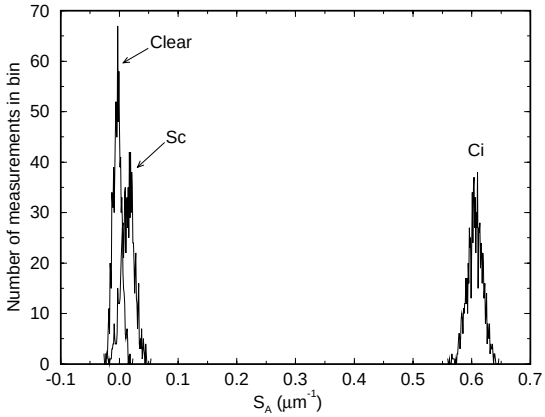

Fig. 6: Frequency distributions of the spectral slope S_A (= $dR_A/d\lambda$) at 1.68 μm for the two cloudy areas and the clear area shown in Figure 4. The corresponding mean spectra are shown in Figures 5a and 5b. Each histogram is made up of 31 × 31 AVIRIS pixels. The bin size is 0.001 μm^{-1}.

In view of the model calculations shown in Figure 3a, the measured slope of about 0.6 μm^{-1} suggests that the optical thickness of the Ci cloud is about 5. Even though this value is dependent on the assumed crystal size (cf. Figures 3a and 3c), the model calculations suggest that the optical thickness is large enough to obtain contrasting values of S_A for the water cloud (or the water surface) and the ice cloud. However, as the optical thickness of the ice cloud decreases this contrast decreases. To illustrate the dependency of S_A on ice cloud optical thickness we derived S_A along transect A (Figure 4), which extends over gradually thickening and thinning Cirrus. Figure 7a shows both S_A and R_A as a function of along-track pixel coordinate (y). The corresponding histogram of S_A is shown in Figure 7b. As for the last figure, there is virtually no overlap between this distribution and the distribution for the Sc field (Figure 6), which confirms the presupposition that the cloud consists of ice crystals. The small values of S_A at the tails of the transect suggest the presence of optically thin Cirrus. The presence of thin clouds is also indicated by R_A itself (Figure 7a); the lowest values are still substantially higher than the background reflectivity, which is less than 0.01 at 1.6 μm (Figure 5b). If we consider R_A as proxy for optical thickness then Figure 5a suggests the presence of a strong signal in S_A with increasing Ci optical thickness. This agrees with the model calculations shown in Figure 3.

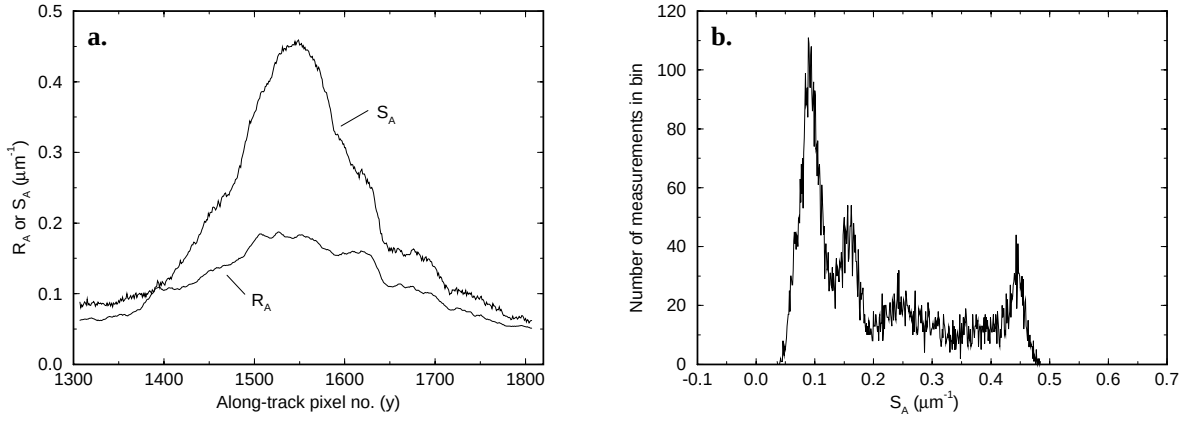

Fig. 7: (a) AVIRIS reflectivity R_A and slope S_A at 1.68 μm for Transect A (see Figure 4). The x-axis represents the along-track pixel coordinate. Each data point represents a 10 pixel across-track mean. The length of the transect is about 10 km (500 pixels). The transect extends over an area of gradually thickening and thinning Cirrus. **(b)** Frequency distribution of S_A.

Compared to Transect A, the situation for Transect B is more complicated because this transect contains areas of both Sc and Ci, and a transitional zone between both cloud types (Figures 4, 8a, and 8b). The first peak in the histogram roughly corresponds to the first 260 pixels of the transect, which covers the Sc field. The rest of the histogram contains several peaks, which correspond to clusters of pixels of different optical thickness (or particle size) in the Ci field. The variation of S_A along the transect suggests a gradual transition from water to ice cloud rather than an abrupt change. In the transitional area the radiative properties of both cloud layers determine the measured slope. It is plausible that a mixture of water droplets and ice crystals in the same cloud can lead to similar values of S_A, as compared to the situation of a two-layered cloud system consisting of optically thin Ci over Sc. Both cases will be referred to as "mixed phase".

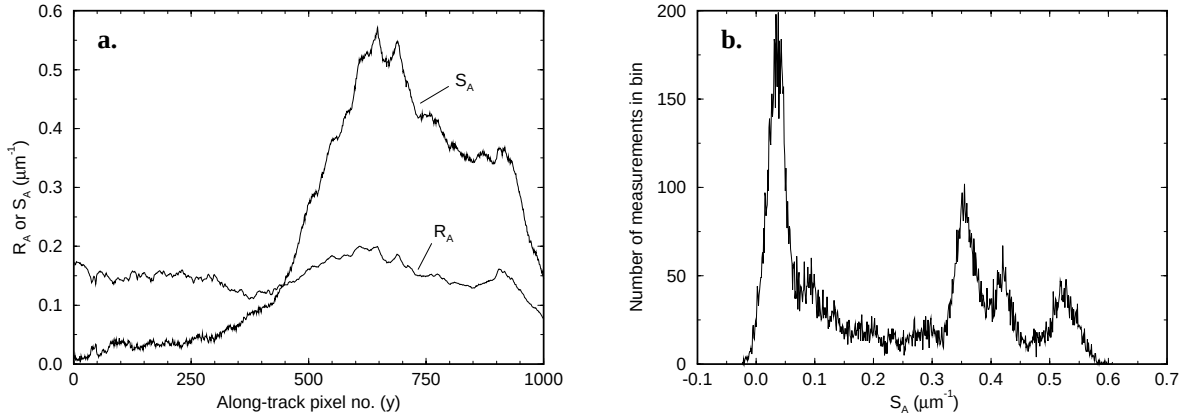

Fig. 8: (a) AVIRIS reflectivity R_A and spectral slope S_A at 1.68 μm for Transect B (Figure 4). The x-axis represents the along-track pixel coordinate. Each data point consists of a 10 pixel across-track mean. The length of the transect is about 20 km (1000 pixels). The first part of the transect extends over Sc, the second over Ci. In between there is an area of optically thin Ci over Sc. **(b)** Histogram of S_A.

3.2 Formulation of water/ice cloud classification scheme

In view of the different cloud types found along Transect B, in this subsection we will formulate a water/ice classification scheme on the basis of the magnitude of the measured spectral slope in the reflectivity at 1.68 μm (S_A). Figure 9 summarizes the classification scheme. For cloudy pixels, three different classes are distinguished: (1) water cloud, (2) mixed phase cloud *or* thin ice cloud, and (3) ice cloud. The ambiguity in the second class refers the fact that both a mixed phase cloud and a thin ice cloud can have similar values of S_A. In order to quantify this class we introduce two thresholds for S_A: T_w and T_i. The second class refers to values of S_A for which $T_w < S_A < T_i$.

To first determine wether a pixel is clear or cloudy, we assume that the surface reflectivity A_s is much smaller than the cloud reflectivity. A pixel is considered to be clear if $R_A \leq A_s$. In the present case of clouds over ocean, this criterion is best fulfilled at a wavelength in the visible, where clouds are bright and the ocean is dark. Note that problems may occur in cases where the surface is highly reflective (e.g. snow, sun glint).

On the basis of the classification scheme shown in Figure 9, and by chosing values of T_w, T_i, and A_s we can arrange the AVIRIS flight line into different classes according to cloud phase. Since $S_A = 0.05\ \mu m^{-1}$ marks the upper limit of the Sc distribution shown in Figure 6, $T_w = 0.05\ \mu m^{-1}$ is a reasonable choice to define the class of water clouds. As an example, we take for T_i twice the standard deviation of the S_A distribution for Sc: $T_i = 0.1\ \mu m^{-1}$. In view of the model calculations shown in Figure 3, this seems to be a workable choice. For A_s we take 0.02. Distributions of R_A (at 0.87 μm) and S_A (at 1.68 μm) for the lowest block of data of the AVIRIS flight line (Figure 4) are shown in Figure 10a and 10b, respectively. The classified image is shown in Figure 10c. We show R_A at a relatively short wavelength to emphasize the contrast between Sc and Ci (cf. Figure 5a). This makes the presence of Ci in the upper right corner of Figure 10a clearly visible. The light-grey to white grey-tones in Figure 10b, which indicate that S_A differs significantly from 0, also clearly mark the Ci field. Consequently, the Ci cloud is well identified by the classification scheme (Figure 10c). Apart from the water and ice clouds, the classified image shows

a relatively large area that was classified as mixed phase cloud. In the present case, this area refers to a two-layered cloud system of optically thin Ci over Sc.

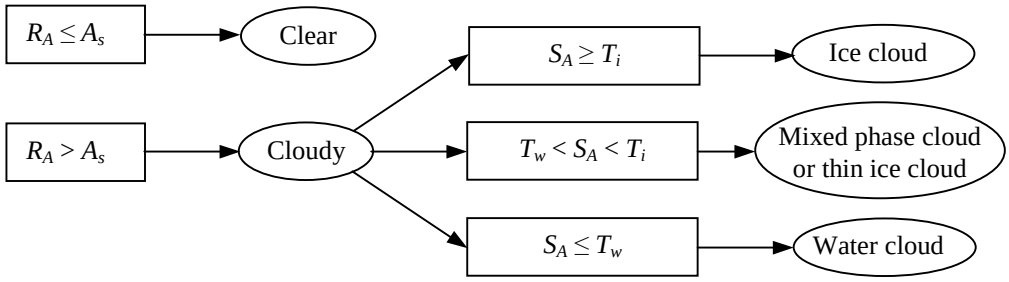

Fig. 9: Classification scheme for water/ice clouds. To determine whether a pixel is clear or cloudy it is assumed that the AVIRIS cloud reflectivity R_A is significantly higher than the surface reflectivity A_s. If a pixel is cloudy then the phase of the cloud is determined on the basis of the spectral slope in the reflectivity S_A at 1.68 μm. For $T_w < S_A < T_i$, classification is ambiguous: the pixel considered can consist of either a mixed phase cloud or an optically thin ice cloud.

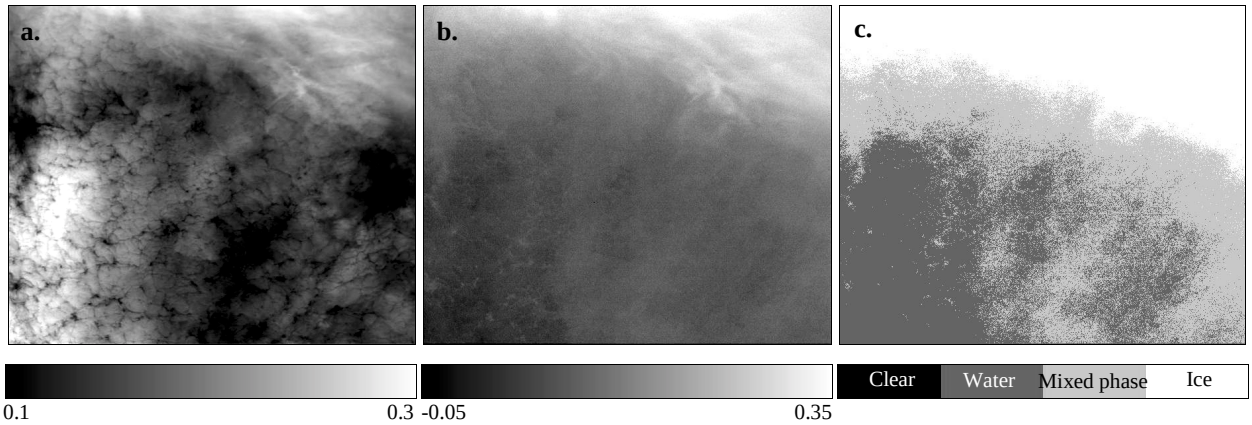

Fig. 10: (a) Reflectivity at 0.87 μm for the lowest block of data shown in Figure 4, **(b)** the slope S_A for the same area, **(c)** the same image arranged in classes according to the classification scheme shown in Figure 9, with $A_s = 0.02$, $T_w = 0.05$ μm^{-1}, and $T_i = 0.1$ μm^{-1}. Note that, according to the scheme, there are no clear pixels present in the image. In this example, the mixed phase area corresponds to optically thin Cirrus over Stratocumulus.

4 SUMMARY AND CONCLUDING REMARKS

On the basis of radiative transfer calculations we expect that characteristic features in the absorption spectra of water and ice show up in near-infrared TOA reflectivity spectra of water and ice clouds. At about 1.68 μm, the modelled spectral slope in the reflectivity S_m equals 0 for water clouds (local maximum in reflectivity). For ice clouds, however, S_m varies between slightly positive values for small optical thickness to roughly 1.5 μm^{-1} for large optical thickness. The difference in slope seems to be more or less independent on solar and viewing geometry, and on cloud particle size. Additional model calculations are needed to confirm this idea.

The difference in the reflectivity spectra of water and ice clouds is used to discriminate between these clouds in an AVIRIS flight line acquired over the Pacific Ocean. This flight line contains fields of both low-level (Stratocumulus; Sc) and high-level (Cirrus; Ci) clouds which, most probably, consist of water droplets and ice crystals, respectively. On the basis of their structure, these cloud fields could easily be recognized in the AVIRIS image. Histograms of the spectral slope in the AVIRIS reflectivity at 1.68 μm, S_A, over selections of optically thick Sc and Ci reveal two distinct and narrow peaks: one at $S_A = 0.01$ μm^{-1} and the other at $S_A = 0.6$ μm^{-1} (no overlap). This implies that model calculations and AVIRIS measurements quantitatively agree, and that the principle of using the shape of the reflectivity spectrum for discriminating between water and ice clouds is basically correct.

As suggested by the model calculations, the AVIRIS measurements show that water and ice clouds are less easy to distinguish from each other as the ice cloud becomes optically thinner. Based on the magnitude of S_A, a classification scheme is presented which makes it possible to arrange cloudy parts of the AVIRIS flight line into three classes: (1) water cloud, (2) mixed phase cloud *or* thin ice cloud, and (3) ice cloud. The ambiguous character of the second class is due to the fact that both a mixed phase cloud and a thin ice cloud can have similar values of S_A. The second class is bounded by two thresholds for S_A. Additional model calculations for mixed phase clouds and multilayered clouds of different phases may provide more insight in the usefulness of these thresholds and their values. Besides, it would be useful to further investigate the role of surface properties (such as spectral reflectivity) in the discrimination scheme.

Even though the classification scheme presented here needs some refinements, the general conclusion is that near-infrared reflectivity spectra, obtained by airborne or spaceborne instruments, provide the information needed to effectively discriminate between water and ice clouds. Measurements made by the satellite instrument SCIAMACHY will cover the spectral range of interest (1.6-1.7 μm) with more than sufficient spectral resolution (~ 1 nm), so the classification scheme presented here should be applicable to global measurements made over clouds.

ACKNOWLEDGEMENTS

Financial support for this research was provided by Space Research Organization Netherlands (SRON project EO-025).

REFERENCES

Bowker, D. E., R. E. Davis, D. L. Myrick, K. Stacy, W. T. Jones, 1985, "Spectral reflectances of natural targets for use in remote sensing studies", NASA reference publication, 1139.

Downing, H. D., and D. Williams, 1975, "Optical constants of water in the infrared", *J. Geophys. Res*., **80**, 1656-1661.

Gao, B.-C., and A. F. H. Goetz, 1993, "Cirrus cloud detection from airborne imaging spectrometer data using the 1.38 μm water vapor band", *Geophys. Res. Let*., **20**(4), 301-304.

Hale, G. M., and M. R. Querry, 1973, "Optical constants of water in the 200 nm to 200 μm wavelength region", *Appl. Opt.*, **12**, 555-563.

Hess, M., R. B. A. Koelemeijer, and P. Stammes, 1998, "Scattering matrices of imperfect hexagonal ice crystals", *J. Quant. Spectrosc. Radiat. Transfer*, **60**(3), 301-308.

Knap, W. H., M. Hess, P. Stammes, R. B. A. Koelemeijer, and P. D. Watts, 1999, "Cirrus optical thickness and crystal size retrieval from ATSR-2 data using phase functions of imperfect hexagonal ice crystals", *J. Geophys. Res.*, **104**(D24), 31,721-31,730.

Mishchenko, M. I., W. B. Rossow, A. Macke, A. A. Lacis, 1996, "Sensitivity of cirrus cloud albedo, bidirectional reflectance and optical thickness retrieval accuracy to ice particle shape", *J. Geophys. Res.*, **101**(D12), 16,973-16,985.

Palmer, K. F., and D. Williams, 1974, "Optical properties of water in the near-infrared", *J. Opt. Soc. Am.*, **64**, 1107-1110.

Pilewskie, P., and S. Twomey, 1987a, "Cloud phase discrimination by reflectance measurements near 1.6 and 2.2 μm", *J. Atmos. Sc.*, **44**(22), 3419-3421.

Pilewskie, P., and S. Twomey, 1987b, "Discrimination of ice from water in clouds by optical remote sensing", *Atmos. Res.*, **21**, 113-122.

Stammes, P., 1994, "Errors in UV reflectivity and albedo calculations due to neglecting polarisation", *Proc. SPIE Int. Soc. Opt. Eng.*, **2311**, 227-235.

Warren, S. G., 1984, "Optical constants of ice from the ultraviolet to the microwave", *Appl. Opt.*, **23**, 1206-1225.

Wiscombe, W. J., and S. G. Warren, 1980, "A model for the spectral albedo of snow. I: Pure snow.", *J. Atmos. Sc.*, **37**, 2712-2733.